Methods for Characterizing the Reliability of Deployable Modules for Large Optical Reflectors

Kristina Hogstrom[1] and Sergio Pellegrino[2]
California Institute of Technology, Pasadena, CA, 91125

The In-Space Telescope Assembly Robotics (ISTAR) project has proposed an architecture for a large robotically-assembled telescope in space, comprised of many deployable truss modules. The truss modules are based on the Pactruss deployment scheme and are equipped with Rolamite tape spring hinges. Fabrication and assembly errors that arise from bulk manufacturing the modules may make the deployment unreliable. A simulation toolkit has been developed to characterize the deployment behavior of the module in the presence of such errors. This paper first outlines the details of the toolkit, including the truss model, the Rolamite hinge model, and the simulation methodology. It then describes the experiment designed to validate the toolkit. A module was constructed and deployed while tracking the displacements of a select node and the rotations of the Rolamite hinges. The measured shape of this module was recreated in the simulation model and the same parameters were obtained. It was found that the experimental and simulated nodal displacements matched within 10%. The experimental hinge behavior was generally captured in the simulation, with some discrepancies in the latching of one hinge. The possible causes for the discrepancies and ongoing work to improve the results are discussed in the paper.

Nomenclature

L	=	deployed module hexagonal side length
H	=	deployed module depth
q	=	folded module side length
d	=	member outer diameter
t	=	member wall thickness
E	=	Young's modulus of member material
ρ	=	density of member material
μ	=	member centerline distance of Rolamite tape spring hinge
p	=	pivot point distance of Rolamite tape spring hinge
$\alpha\pi$	=	critical angle of Rolamite hinges
t_{latch}	=	switch variable defining Rolamite hinge profile
M	=	moment provided by tape spring hinge
θ	=	rotation of tape spring hinge
n	=	number of cases
R	=	reliability

I. Introduction

FUTURE astronomical studies will require extremely large optical space telescopes in order to image Earth-sized exoplanets or study the first stars. There is an inherent size constraint for large primary apertures in space, posed by launch vehicle payload fairings, which can be bypassed by in-space assembly. Feasible assembly strategies can be achieved with a modular approach, dividing the support structure of the optical reflector into a series of repeating truss modules that fold compactly for launch and are deployed and connected on orbit by a robot. Optical telescopes require precision on the level of nanometers, and while the use of active optics can relax this tight tolerance, the deployable

[1] Graduate Student, Graduate Aerospace Laboratories, MC 205-45. AIAA Student Member.
[2] Joyce and Kent Kresa Professor of Aeronautics and Professor of Civil Engineering, Graduate Aerospace Laboratories, 1200 E. California Blvd, MC301-46. AIAA Fellow.

modules must be able to reliably unfold to the correct shape in order to avoid distortions in the assembled structure. Even small fabrication errors in the truss module members may compound to hinder deployment. Deployment reliability is thus an important parameter that must be quantified in order to establish the feasibility of the mission.[1] In this context, reliability is defined as the percentage of modules with unique error distributions that deploy completely without any kind of failure (e.g. hinge failing to latch or a node largely out of place).

One architecture for a large modular optical reflector utilizes the assembly robot to deploy simple and passive modules equipped with Rolamite tape spring hinges.[2] The deployment scheme of the module is based on the Pactruss developed by Astro Aerospace Corporation and NASA Langley Research Center.[3] To optimize the design of the module, the following questions must be answered:

- How do design parameters, such as member diameter, hinge stiffness, wall thickness, and material, affect deployment reliability?
- What kinds of errors, such as member length errors and joint misalignments, are most detrimental to deployment reliability?

A purely experimental approach to answering these questions would entail the building and testing of hundreds of modules with varying error distributions to obtain a statistically significant reliability estimate. This costly and time-consuming process can be mitigated with an approach based on numerical simulations. In this research, a simulation toolkit has been developed, using a combination of Python and the finite element software package Abaqus, that can reproduce the deployment behavior of a Pactruss module in the presence of errors. This paper outlines the details of the toolkit, starting with the simulation model, which includes the complicated nonlinear behavior of the Rolamite hinges. Possible types of errors that may be present in a physical module are discussed, as well as how those errors can be included in the simulation model.

This paper also describes the experiment performed to validate the simulations. Two modules were built to the same nominal specifications. Their precise shapes were measured, yielding bounds on the magnitudes of errors that may be introduced by this manufacturing process. One module was then attached to a motor that actuated a slow, controlled deployment. Select nodal displacements and hinge rotations were measured. The actual shape of the module was reproduced in the simulation model, and the experimental measurements were compared with simulation results. The comparison showed good agreement in nodal displacements but some discrepancies in hinge rotations. Further work is being done to build more fidelity into the model.

Once the experimental validation is satisfactory, the toolkit can be used to simulate the deployment of many unique modules with errors randomly selected from distributions bounded by realistic manufacturing specifications. The geometric parameters of the module, the types and magnitudes of errors applied, and the deployment method can be easily adjusted to perform extensive trade studies and optimize the design. Though only the Pactruss module is considered in this research, any deployable truss geometry can be analyzed simply by specifying the endpoints of the members and the behavior of the joints. Thus, the toolkit can provide critical reliability estimates for any large-scale modular assembly mission.

II. Structure Details and Simulation Toolkit

A. Truss Module

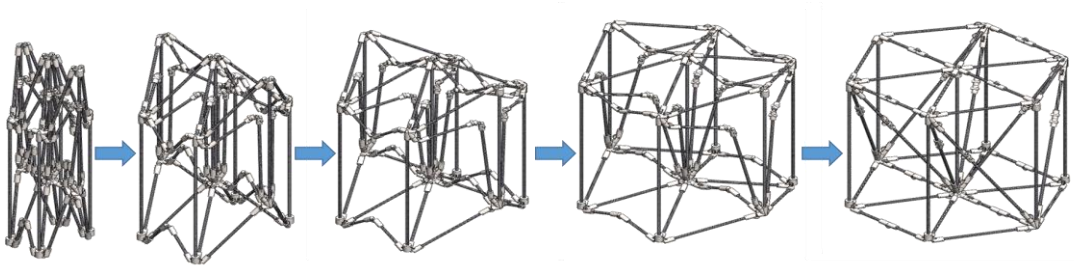

Figure 1. Pactruss module deployment

A Pactruss module has 39 members in total, of which 16 fold in the middle. Each mid-member hinge is a Rolamite tape spring hinge, with properties discussed in Section IIB. In the stowed configuration, the module resembles a folded umbrella, with joint offsets that allow every member to be vertical. A diagram of the deployment is shown in Figure 1. A robot deploys the module by holding two opposing vertical members and controlling the rate at which they move apart. The module can self-deploy with only spring actuation, and so the robot works against the tape spring hinges for a slow, quasistatic deployment.

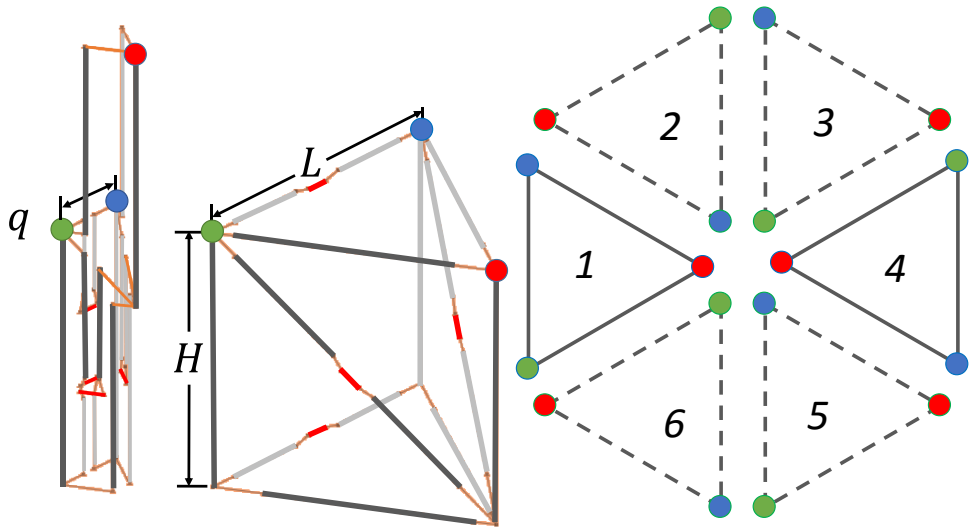

Figure 2. From left to right: 1/6th wedge section in folded configuration, 1/6th section in deployed configuration, tessellation of 1/6th sections to recreate full module. Dashed outlines indicate that the section is mirrored with respect to a horizontal plane.

The module behavior can be initially studied by considering a 1/6th "wedge" section, which is tessellated as shown in Figure 2 to recreate the full hexagonal module. L is the side length of the deployed module, and H is the depth of the deployed module. The dimension q is the side length of the folded module, a measure of the stowage profile compactness. In the figure, the tape spring hinges are marked in red.

Dimensions not shown include:

- d, the outer diameter of the tubular members,
- t, the wall thickness of the members,
- E, the Young's modulus of the member material,
- and ρ, the density of the member material.

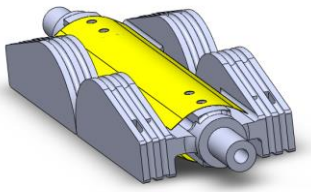

Figure 3. Rolamite tape spring hinge.

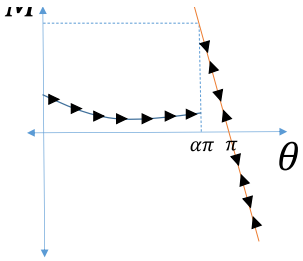

Figure 4. Approximate moment-rotation curve of a Rolamite tape spring hinge. The pre-latching region is shown in blue and the latching region in orange.

The finite element software package Abaqus/Standard is used for all simulations.[4] In Abaqus, the members are modeled as beam elements. Joint offsets (shown in orange in Figure 2) are created using rigid beams that are fixed to the vertical member on one side and connected with a revolute pin joint (1 rotational DOF, no elasticity) to the other member on the other side. The model of the Rolamite tape springe hinges is described in Section IIB. Factors like gravity and joint masses are included as necessary to recreate physical scenarios. At this time, friction and compliance in the joints are assumed to be negligible.

B. Rolamite Tape Spring Hinge Model

A Rolamite tape spring hinge, shown in Figure 3, consists of a pair of steel measuring tape sections attached to four circular cams that are restrained to roll on each other, allowing only one rotational degree of freedom. They can fold compactly and then snap into a stiff configuration upon unfolding. The approximate moment-rotation profile of a Rolamite hinge is shown in Figure 4. It is divided into two regions: pre-latching and latching. The rotation angle θ is defined to be 0 when the hinge is completely folded and π when it is completely unfolded. As the hinge unfolds and θ increases, the moment follows the curve defined by the pre-latching region. When the critical angle $\alpha\pi$ (in radians) is reached, where α is a constant close to unity, the moment jumps to a much higher value (~three orders of magnitude) then decreases along a line to 0 when $\theta = \pi$ radians. Kinetic energy may rotate the hinge beyond $\theta = \pi$, at which point the moment becomes increasingly negative, driving the hinge back to the unfolded

state. The hinge may continue to oscillate around $\theta = \pi$, but the moment will still follow the linear profile that defines the latching region until any remaining kinetic energy is damped.[5]

Figure 5 shows the kinematic model of the Rolamite hinge. The two key dimensions are p, the distance between the centers of the circular pieces or twice the radius of curvature, and μ, the distance between the attached member centerlines when the hinge is folded. Other dimensions that affect the hinge behavior include the distance between the edges of the tape sections and the length of the tape sections between the attachment points. The hinge is modeled by creating nodes a_1 and b_1, where the member centerlines attach to the Rolamite pieces, and coincident nodes a_2 and $a_2{}'$ at the center of one curved section and b_2 and $b_2{}'$ at the center of the other curved section. In Abaqus, the degrees of freedom of two nodes are linked with connectors. Hinge connectors create a simple 1-DOF hinge between two nodes with an axis of rotation defined by setting a local coordinate system. Two hinge connectors link a_2 to $a_2{}'$ and b_2 to $b_2{}'$ respectively. The rotations of the connectors are defined to be equal in magnitude and opposite in sign. Rigid beams connect a_1 to a_2, $a_2{}'$ to $b_2{}'$, and $b_2{}'$ to b_2.

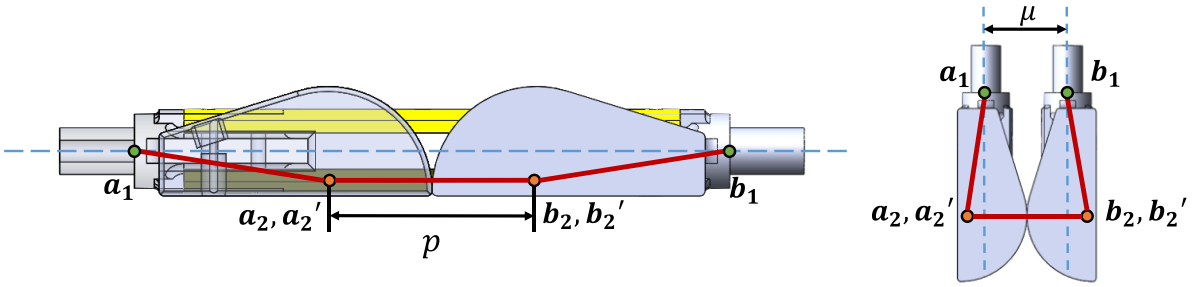

Figure 5. Rolamite tape spring hinge kinematic model.

The moment-rotation behavior of the hinge connectors can be described as a piecewise function based on a switch variable t_{latch}, such that the pre-latching portion of the profile is followed when t_{latch} is equal to 0 and the latching portion is followed when t_{latch} is equal to 1. The switch in t_{latch} occurs the first time the rotation in the connector exceeds the critical angle $\alpha\pi$ and remains unchanged thereafter. This behavior is simulated in Abaqus by defining the moment as a function of the rotation angle θ and the field variable t_{latch} with a lookup table. Two customized user subroutines that run in parallel to Abaqus are required to set the value of t_{latch}: URDFIL and UFIELD. At the beginning of the simulation, t_{latch} is initialized to zero. After every time increment, URDFIL extracts the θ value of each connector and feeds it to UFIELD, which determines whether $\theta > \alpha\pi$. Once this criterion is true, UFIELD sets t_{latch} to 1, and Abaqus is signaled to follow that section of the moment table for the remainder of the simulation.

C. Possible Error Types

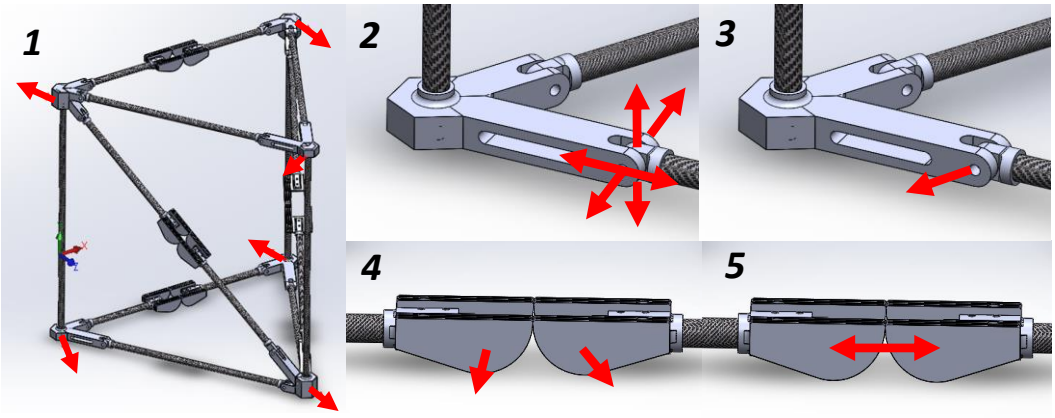

Figure 6. Graphical depiction of error types.

There are many ways in which the geometry and behavior of a physical module may deviate from the nominal design. In the toolkit, the following error types may be included:

1. Node offsets: translation of nodes in *x*, *y*, and *z* directions.
2. Pin offsets: translation of pin locations in *x*, *y*, and *z* directions.
3. Pin misalignments: non-zero angle between actual pin axis and nominal pin axis.

4. Tape hinge alignment errors: non-zero angle between the normals of the two Rolamite halves.
5. Tape hinge centerline errors: value of p different from nominal.
6. Tape hinge moment profile errors: moment provided by hinge at a given angle different from nominal.

The error types 1-5 are graphically depicted in Figure 6 and the coordinate system in Figure 7. While all of these error types may be included in the model, only the node and pin offsets have been tested at this time.

D. Simulation methodology

The first step in the simulation is to create the model in the stowed configuration by specifying the endpoints of each member and the connectivity matrix, denoting which connections are Rolamite hinges and which are revolute pin joints. Errors can be prescribed or drawn from a random uniform distribution, with bounds representative of realistic magnitudes for each error type. These errors are built directly into the member endpoint and joint axis definitions, meaning the simulation has no knowledge of a nominal shape. Connectors are defined to span the gap between the endpoints they connect, even if the endpoints include errors. This means that there are no conflicting dimensions and the model is unstressed at the start of the deployment, with the exception of the moments exerted by the Rolamite hinges. Construction of physical modules required little force to connect the members, suggesting that stresses caused by misalignments were negligible. Thus it is reasonably assumed that such stresses can be ignored in the model.

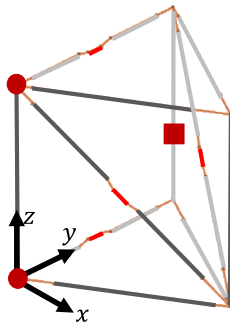

Figure 7. Location of fixed nodes (circles) and controlled node (square).

The module is deployed by imposing a displacement boundary condition on a controlled node. In Figure 7, the nodes marked with red circles are fully fixed. In a static step, the node marked with a red square is moved along the y-axis for either a set distance or until the net reaction forces in the y-direction at the fixed nodes are in tension. For a module without errors, the distance to reach full deployment is $L - q$. To mitigate the instabilities associated with the discontinuity in the Rolamite hinge moments, Abaqus is set to employ an automatic stabilization procedure that artificially damps any large local velocities that may arise. The amount of applied damping is proportional to the extrapolated strain energy released by the instability. The default proportionality constant in Abaqus is 2×10^{-4}. For these simulations, it was found by trying constants in the range of 10^{-12} to 10^{-4} that a value of 6×10^{-9} was sufficient to remove instabilities and complete the simulation without numerical errors.

E. Simulation results

As an example of the simulation results, Figure 8 shows some stages of the controlled deployment of a model without any errors, such that the nodes and members form a perfect triangular prism and all pin and hinge axes are aligned with the face normals. For this example, $L = H = 50$ cm and $q = 13$ cm. The previously described boundary conditions are applied, meaning that the controlled node, marked with a square, is moved a distance of $L - q$ along the y axis. Figure 9 shows the displacement of the node marked with a circle in Figure 8, as a function of the displacement of the controlled node. This node is particularly useful for visualizing deployment behavior, because it has bulk motion in all three directions. Figure 10 shows the rotations of the four Rolamite hinges as they move from fully folded ($\theta = 0°$) to fully unfolded ($\theta = 180°$). It is evident from the inset that the two diagonal hinges latch at the same time, followed by the bottom folding longeron and the top folding longeron in close succession.

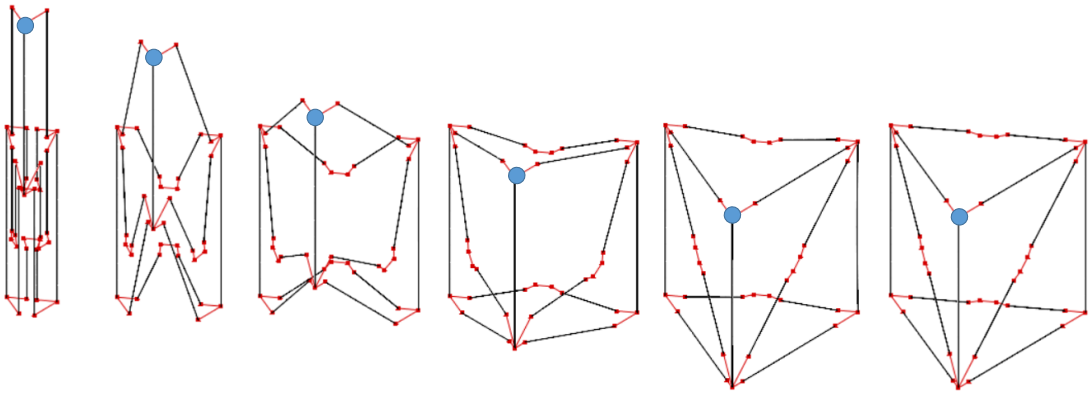

Figure 8. Stages of simulated controlled deployment.

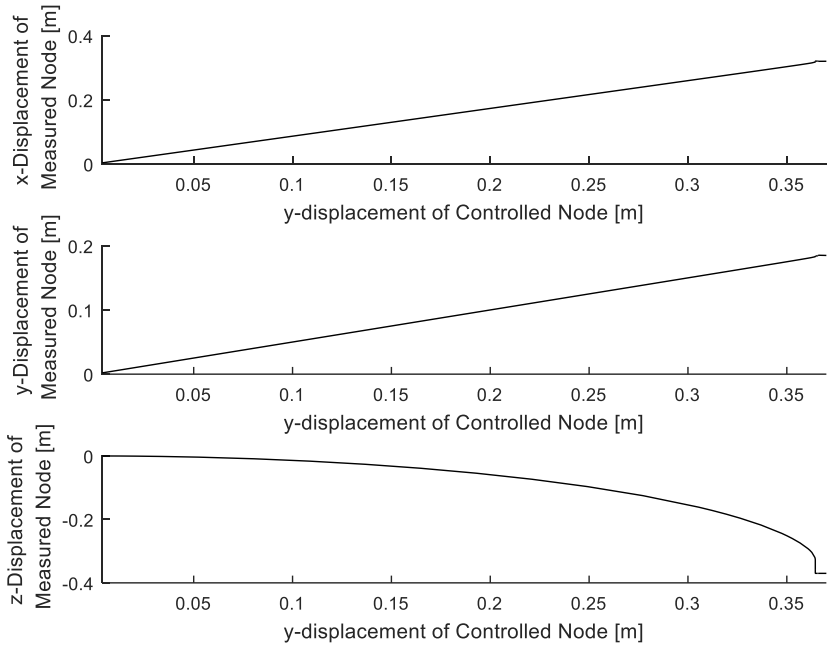

Figure 9. *x, y,* and *z* displacements of node in Figure 8 vs. *y* displacement of controlled node.

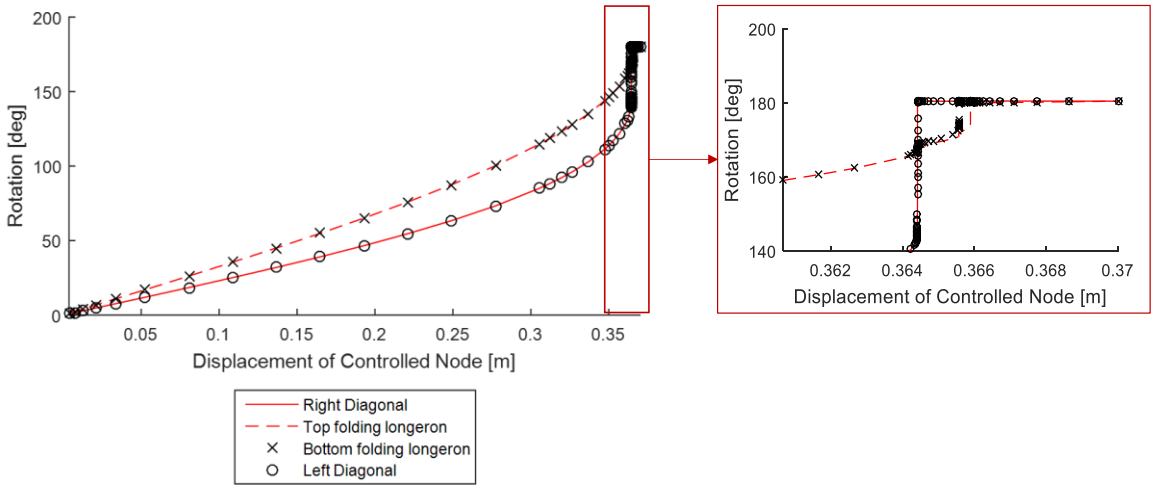

Figure 10. Rotations of the four tape spring hinges shown in Figure 8. Right inset magnifies the final stages of deployment.

F. Reliability Estimation

To estimate the reliability of deployment, a set of analyses are performed, each simulating the deployment of one module with a unique randomly chosen error distribution. The simulation is determined to be a success if all of the following criteria are met at the end of the deployment:

- All tape hinges are fully latched (have reached full rotation).
- All nodes are within a set tolerance of their nominal position, as defined by the mission constraints.
- The reaction forces during deployment are within a tolerable level, as defined by the mission constraints.

For n simulations in the analysis set, where $n \geq 50$ for statistical significance, the percentage of simulations marked as successful, or the reliability R, is recorded, with confidence interval $R \pm 1.96\sqrt{\frac{1}{n}R(1-R)}$.[6]

III. Experimental Validation

A. Experimental Model

Experimental validation was required to ensure that the simulations adequately capture realistic deployment behavior. Two key quantities were used as comparison measures between simulations and experiments: nodal displacements and Rolamite hinge rotations. This section describes the experiment model, measurement techniques, and the validation results.

1. Truss geometry

Two physical modules were built from carbon fiber composite rods and 3D printed ABS plastic joints. The nominal dimensions for both modules were the same and are given in Table 1. In order to draw an appropriate comparison between simulations and experiments, the actual, rather than nominal, geometry of the modules needed to be reproduced as closely as possible in the simulation model. A specific kind of coordinate measurement machine called a FaroArm was used to measure the shape of both modules, including the locations of the six nodes, the offsets from the nodes of the 16 pins, and the axes of the 16 pins. The same measurements were made for both the stowed and deployed configurations. Figure 11 shows, for the deployed module, the average and maximum errors in these measurements from the nominal, as well as the deformed shape superimposed on the nominal shape. The results in Figure 11 provide statistical data on the magnitudes of errors introduced in this manufacturing process, and will be used as the basis for reliability studies in the future. However, it should be noted that the errors include not just fabrication errors in the module, but also measurement errors by the FaroArm. The FaroArm itself has a precision on the level of tens of micrometers, but the act of touching the arm to the module deformed the module slightly, yielding a measurement error that was observable but not quantified.

Table 1. Dimensions of experimental model.

E	150 GPa
ρ	1820 kg/m^3
L	50 cm
H	50 cm
q	13 cm
d	1.1303 cm
t	0.889 mm

The deployed shape is shown because it is of greatest practical interest. However, the simulation model was constructed in the stowed position using only the stowed position measurements. At this time, only the measured node and pin locations were recreated in the simulation model. The pin orientations were kept at the nominal value, normal to the corresponding face of the perfect triangular prism. Both modules were measured to obtain a larger statistical sample size, but only the second module was used in the experiments presented in this paper. The mass of each joint was also measured and included in the model, with gravity applied in the direction that matches the experimental scenario.

	Average Error	Maximum Error
Node locations	1.89 mm	7.07 mm
Pin locations	0.55 mm	1.73 mm
Pin orientations	0.77°	1.49°

	Average Error	Maximum Error
Node locations	0.86 mm	2.73 mm
Pin locations	0.92 mm	3.27 mm
Pin orientations	1.23°	3.84°

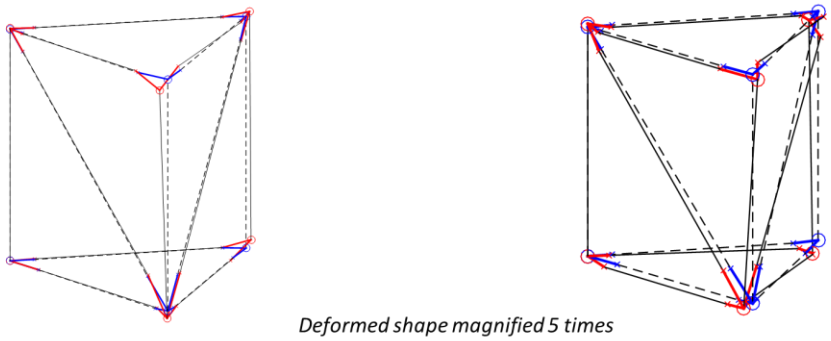

Figure 11. FaroArm measurement results for module 1 (left) and module 2 (right). The nominal shape is shown with blue joints and dashed members, while the actual shape is shown with red joints and solid members.

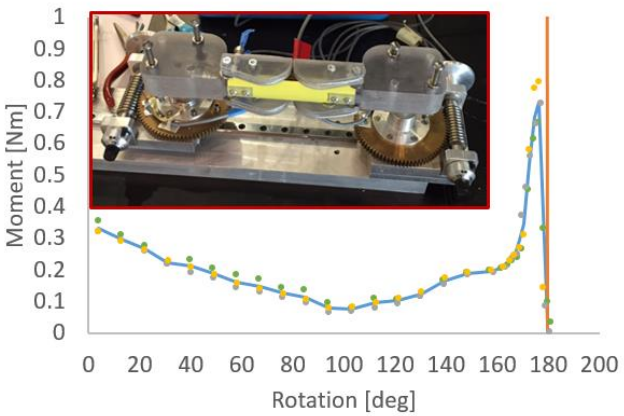

Figure 12. (Blue) experimentally determined moment-rotation curve of a Rolamite tape spring hinge. (Orange) Analytically estimated latching curve that could not be captured by experimental resolution. (Inset) experimental measurement system.

2. Rolamite tape spring hinges

The four Rolamite hinges in each module were constructed with the same nominal dimensions. The tape sections were commercially obtained and the design dimensions were chosen to minimize the size of the hinge while maintaining a radius of curvature large enough to avoid damage. The tape sections were 7 cm long between attachment points, separated by a maximum distance of 1.33 cm. The distance between the centers of curvature, p, was 4.2 cm, while the distance between member centerlines, μ, was 2.6 cm. The moment-rotation profile of one hinge was experimentally measured by attaching each end to a gear, such that a rotation of the gears caused a rotation in the hinge, as shown in the inset of Figure 12. The gears were equipped with strain gauges to measure the moment imparted by the hinge. From the fully folded position, the rotation of the hinge was incremented and the moment at each increment recorded. Three tests were performed, as shown by the markers in Figure 12. The angle corresponding to each increment was approximately, but not exactly, the same for the three tests, meaning that each increment has three angle data points and three moment data points. The average curve shown in blue is comprised of the mean angles and mean moments for every increment. The average standard deviation of the three angle measurements across all increments was 0.45°, which gives a sense of the resolution of the measurement. Similarly, the average standard deviation in the moment was 0.03 Nm.

This experimental method did not have high enough resolution to fully capture the latching region; this was instead estimated analytically using methods discussed in Ref. 5. This analytical curve is shown as the orange line in Figure 12. In the model, the moment discontinuously jumps from the peak of the blue curve at a critical angle of $\alpha\pi = 176.5°$ to the moment on the orange line that corresponds to the same rotation.

Even when the physical module was fully stowed, the hinges were slightly open due to misalignments and gravity sagging. For instance, the largest initial angle was approximately 2.5° in the left diagonal hinge. The initial angles were measured and the applied moment-rotation curve was shifted accordingly in the model, so that the rotation still started at 0° at the start of the simulation but the critical angle decreased. The shift was then removed for plots so that $\alpha\pi$ was consistent for each hinge.

B. Experimental Setup

In the experiment, the second of the two modules measured with the FaroArm was attached to a frame, as shown in Figure 13. Two points on one vertical member were rigidly fixed to the frame, with load cells in line to measure reaction forces in the y axis. The other vertical member on the face with the folding longerons was fixed to a carriage, which moved along a lead screw driven by a motor. The motor operated until the net reaction force registered by the load cells were in tension. This translated to a carriage displacement of about 37 cm, the value of $L - q$.

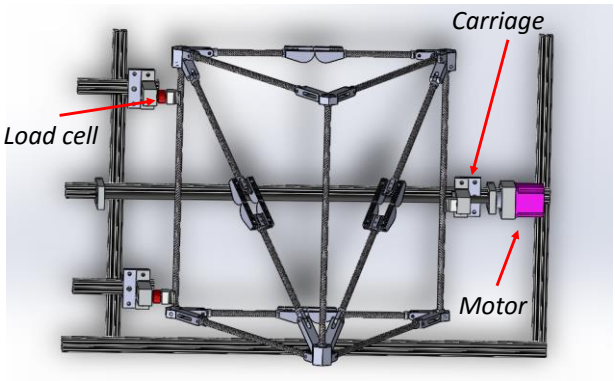

Figure 13. Experimental rig design.

The displacements of select nodes were measured in 3D space by tracking fiducials on the module and frame with stereo camera pair, as shown in Figure 14. Markers 3, 4, and 5 were used to establish the coordinate system, with 3 defining the origin, 5 defining the y-axis, and the three points defining the y-z plane. Marker 5 was attached to the carriage, and thus its displacement in the y-direction controlled the deployment.

The hinge angles were estimated from videos, starting at a carriage displacement of roughly 30 cm, 7 centimeters from the end of the deployment. Only this stage was captured to minimize rigid body movement that may skew the angles. These videos were synchronized so that the time at which each hinge latched could be determined. Angles were extracted from the videos by first manually selecting the endpoints of the Rolamite section edges for a sparse number of frames and interpolating to compute approximate slopes of the edges for each frame. Then, for every frame, Hough transforms were applied to automatically detect any edges.[7] The edges of the Rolamite sections were thus the detected edges with slopes closest to the manual approximations. To estimate the precision associated with this process, each hinge was observed at a constant angle for some time. The angle was computed for each frame, yielding a mean and standard deviation. For the four angles and four tests, the maximum standard deviation was $0.91°$.

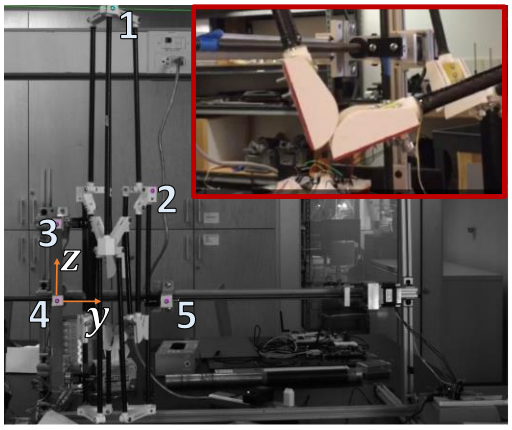

Figure 14. Nodal displacements tracked with a stereo camera pair. (Inset) Hinge angles when tracking begins.

C. Results

Figure 15 shows snapshots of the deployment during experiments. At stage 1, the module was fully folded and the motor began displacing the carriage along the y-axis. The two vertical members on the back face moved apart from each other, while the closer vertical member, starting from a high position, came downward and outward in the $-z$ and $+x$ directions. At stage 6, the diagonal Rolamite hinges latched in quick succession, with the left hinge latching slightly ahead of the other. In stage 7, the lower longeron hinge latched. Finally, in stage 8, the upper longeron hinge latched and the module reached full deployment. Similar behavior was observed in each of four experiments performed.

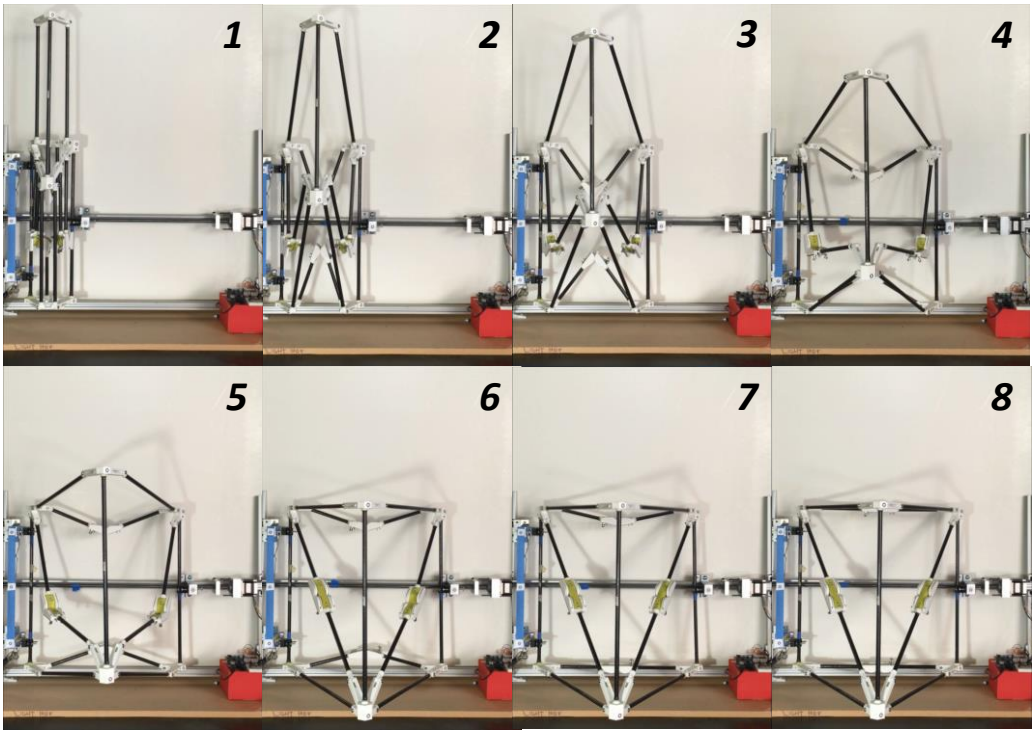

Figure 15. Stages of deployment experiment.

1. Hinge angles

Each plot in Figure 16 shows the rotations of all four hinges in one test, plotted against the displacement of the controlled node. The hinges are labeled according to how they appear in Figure 15. A hinge is latched when the rotation reaches approximately 180° and becomes constant. This plot clearly shows that that two diagonal hinges generally followed the same path until just before latching. The left diagonal hinge latched first. This action forced the right diagonal hinge to suddenly open to an intermediate value, highlighted by the blue dashed line, and maintain this value for a short time. For the four tests, this value was 168° ± 1°. Eventually the right diagonal hinge did latch, followed by the lower longeron hinge and then the upper longeron hinge.

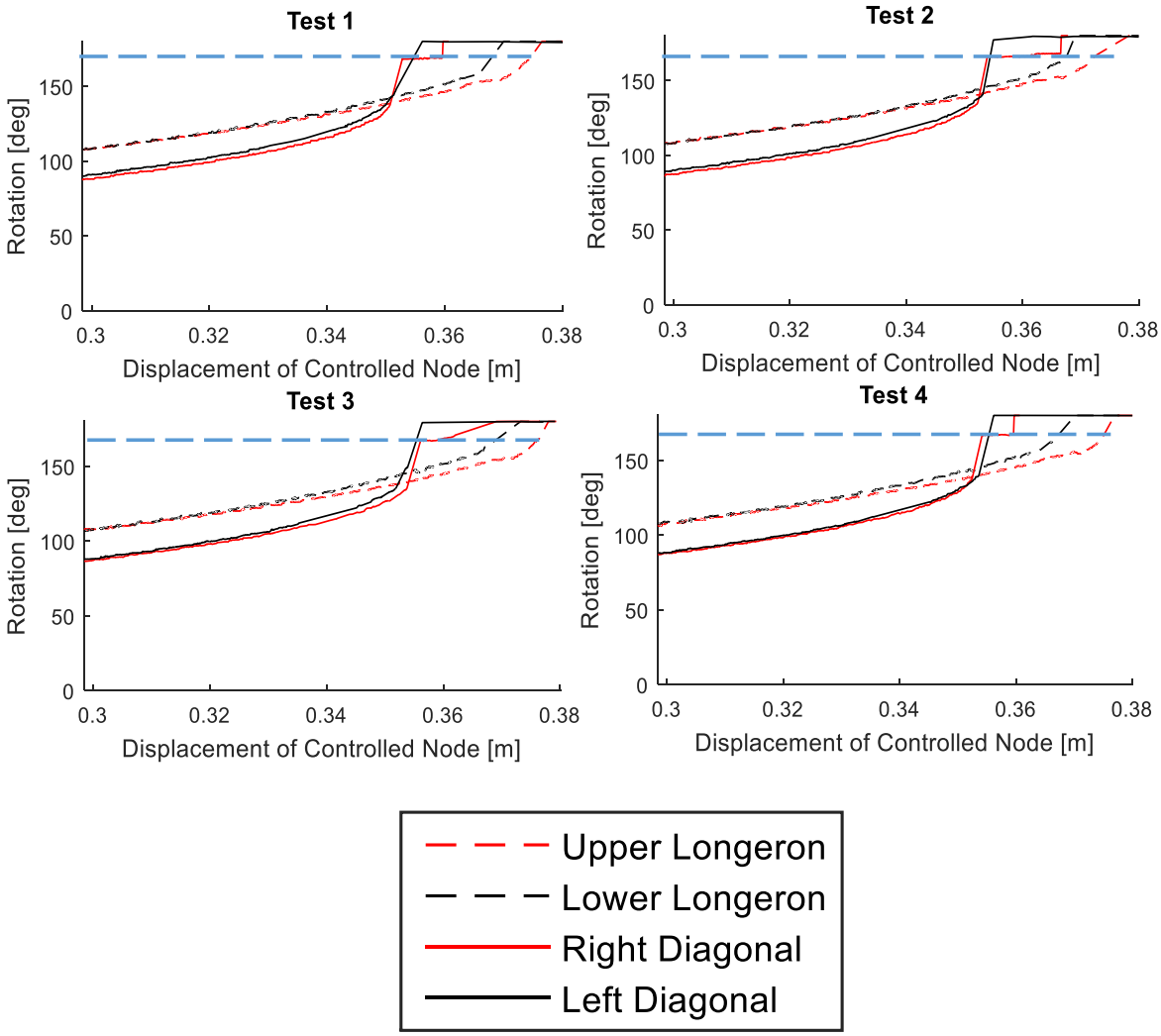

Figure 16. Rotations of Rolamite hinges for four tests. The blue dashed line highlights the steady portion of the right diagonal hinge prior to latching.

Each plot of Figure 17 shows the rotation of one hinge for all four tests, the simulation of the actual measured module, and the simulation of the perfect module, or one with the nominal design parameters. The results show generally good agreement between experiments and the measured module simulation, with two notable discrepancies. First, the upper and lower longeron hinges tended to latch later in the experiments than in the simulation. Secondly, the simulation predicted that the left diagonal hinge would not latch, but rather stay at approximately 164.3° for the remainder of the deployment. The simulation of the perfect module does more closely match the longeron experimental results, but is further from the left diagonal hinge results and does not capture the pre-latching behavior of the right diagonal hinge.

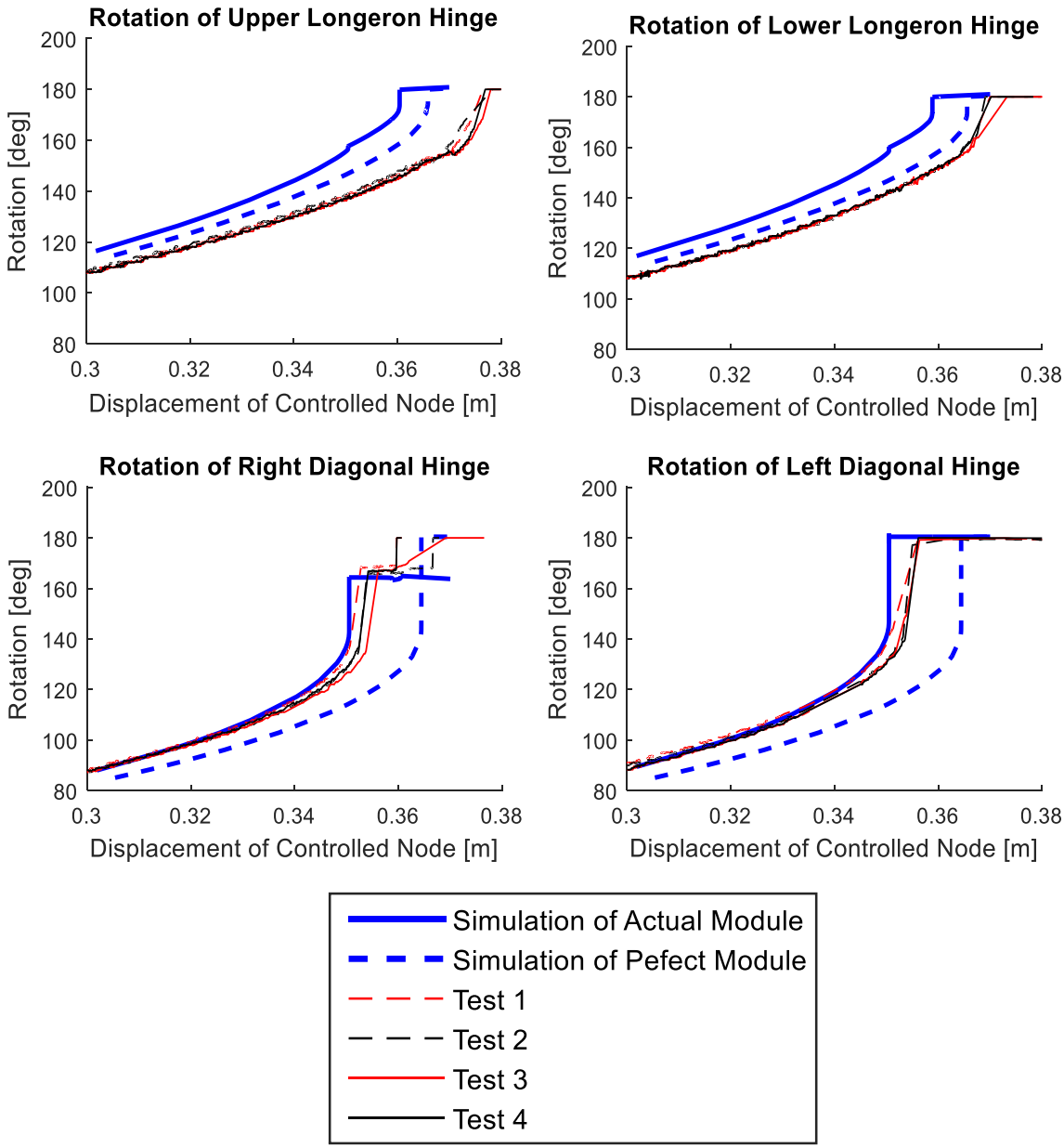

Figure 17. Rotations of each of the Rolamite hinges for the four tests and simulation.

2. Nodal displacements

In Figure 18, the x, y, and z displacements of marker 1, as designated in Figure 14, are plotted against the y displacement of marker 5 for four experiments. On the same axes, the displacements of the corresponding nodes in the simulations of both the actual module and the perfect module are plotted. The results show generally good agreement between experiment and actual module simulations, matching within 10% at the end of the deployment. Both of these data sets show how displacements in the x and y directions are roughly linear, whereas displacement in the z direction increased exponentially. Once the diagonal hinges latch or reach their final rotation, this node becomes roughly fixed in place, as evidenced by the short constant region toward the end of the deployment. Discrepancies in the actual module simulations and the experimental data toward the end of the deployment are likely coupled to the aforementioned discrepancy in the latching behavior of the right diagonal hinge. However, it is especially clear in the z displacement that the simulation of the actual module is an improvement over the simulation of the perfect module.

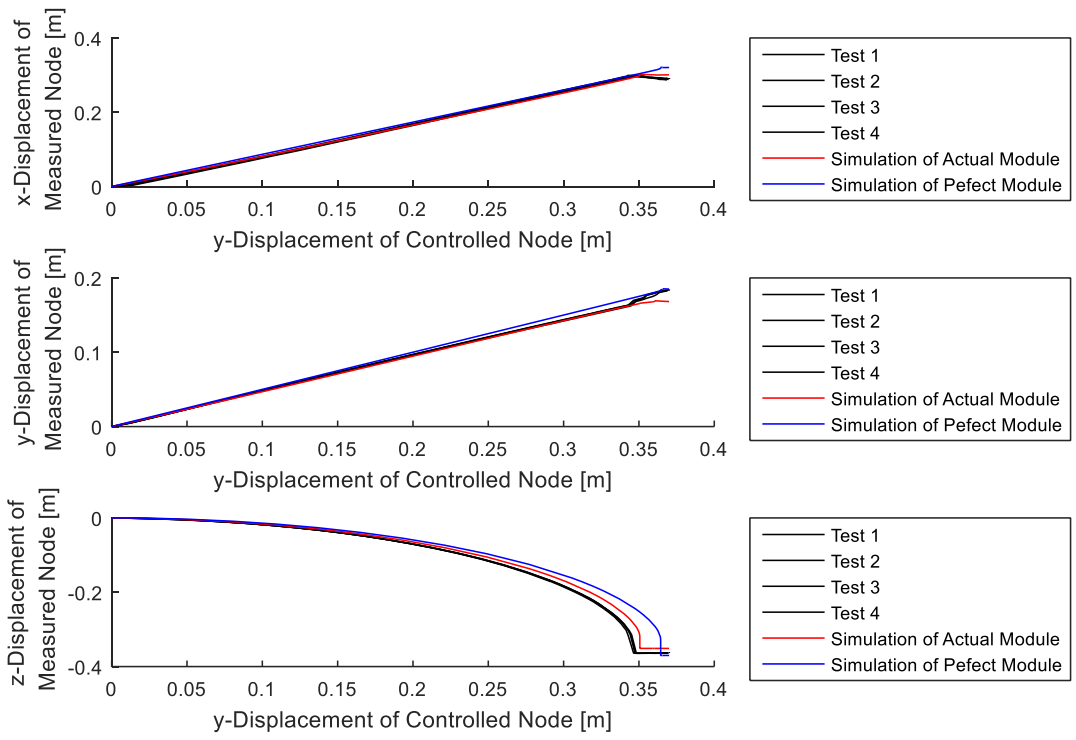

Figure 18. Experimental displacements of marker 1 as defined in Figure 14 and simulated displacements of the corresponding node.

IV. Discussion and Conclusion

For any in-space assembly mission that features many deployable truss modules, deployment reliability despite fabrication and assembly errors is an important mission constraint. This paper has described a simulation toolkit that can estimate reliability by modeling the deployment of a truss module with a random set of errors, categorizing the deployment as a success or failure, and repeating to obtain the percentage of successes. Errors can be drawn from a distribution with bounds set by the tolerances of the manufacturing process. The toolkit has the capability to model any deployable truss geometry by simply specifying the endpoints of the members and the behavior of the joints. Accepted types of joints include simple inelastic revolute pins, linearly elastic springs, and nonlinear and discontinuous Rolamite hinges. In this paper, the toolkit was explained in the context of a Pactruss module with four Rolamite tape spring hinges. The truss model, hinge model, methodology, and possible error types were described.

In order to determine whether the simulation toolkit produces realistic results, experimental validation is required. Thus, a key part of this work was to reproduce an experiment in simulations and compare the results. A physical module was built and its shape measured. In a slow, controlled deployment, the displacements of select nodes and the rotations of the Rolamite hinges were tracked. The same experimental scenario with the measured shape of the physical module was simulated and the same quantities were recorded. The results showed that the simulation of the measured module more closely matched the experimental results than the simulation of the perfect (nominal) module, demonstrating that small errors in the geometry do make a difference in the deployment behavior. The experimental and simulated nodal displacements of the measured module matched within 10% throughout the deployment. The experimental and simulated hinge rotations also matched well for three of the four hinges. The remaining hinge did not latch in the simulation, but reached and held a constant rotation of 164.3°. In experiments, this hinge did latch; however, a constant region at an angle within 2% of 164.3° was captured. The order in which the hinges reached their maximum rotation was also correctly predicted.

The slight but notable discrepancy in the behavior of the one hinge could be caused by many factors. Two possibly significant considerations neglected in the simulation model are joint friction and compliance, which are very difficult to measure as they depend on exactly how tightly the revolute joints were bolted. Other factors include errors in the analytically estimated latching moment of the hinges and in the FaroArm measurements of the module. If the FaroArm

measurements were slightly incorrect, then the simulation model did not exactly match the experimental model, and such discrepancies could arise. Indeed, it was observed that decreasing the lengths of the two members attached to the right diagonal hinge by only 2 mm in the simulation model led to complete latching of that hinge. This shows that the simulations are sensitive to changes in geometry. This sensitivity may be realistic; the purpose of the toolkit is to capture how these small errors affect the deployment. To improve upon the model in the future, the physical module will be remeasured with the FaroArm several times to obtain a statistical estimate of its shape. This new shape will be applied to the simulation model, and it will then be determined whether the predicted results more closely match the experimental results. Other attempts to increase the fidelity of the toolkit, such as experimentally determining the latching moment of the hinges with a four-point bending test, are ongoing. Also, error types besides node and pin locations, such as pin orientations and Rolamite hinge orientations, will be added to the model. The toolkit will be considered validated once the experimental latching behavior of all four hinges is captured.

Once experimentally validated, this toolkit will be used to investigate important questions about the reliability of the deployment, such as how the geometric parameters of the module affect the reliability, and whether certain kinds of errors have a worse effect than others. In this paper, FaroArm measurements of the two modules provide error distributions for that specific geometry and construction method. The next steps in this research are to define random distributions of errors based on these measurements, apply them to the simulations, and estimate the reliability. Then the module geometry and deployment scheme can be adjusted to develop a suite of reliability trade studies that will enable the selection of an optimal design.

Acknowledgments

This work was supported by the NASA Space Technology Research Fellowship #NNX13AL67H, with the help and mentorship of Erik Komendera, John Dorsey, and Bill Doggett at NASA Langley Research Center and Stuart Shaklan at the Jet Propulsion Laboratory. Many thanks to Isabelle Phinney for her help with setting up experiments.

References

[1]Macdonald, M., and Badescu, V., eds., *The International Handbook of Space Technology*, Springer, 2014.

[2]Hogstrom, K., Backes, P., Burdick, J., Kennedy, B., Kim, J., Lee, N., Malakhova, G., Mukherjee, R., Pellegrino, S., and Wu, Y.-H., "A Robotically Assembled 100-meter Space Telescope," *65th International Astronautical Congress*, Toronto, CA: 2014.

[3]Hedgepeth, J. M., *Pactruss support structure for precision segmented reflectors*, Carpinteria, California: Langley Research Center, 1989.

[4]SIMULIA Abaqus, Dassault Systemes, Software Package, Ver. 6.13-2, 2013.

[5]Watt, A. M., "Deployable structures with self-locking hinges," University of Cambridge, 2003.

[6]Lane, D. M., "Confidence Interval on a Proportion," *Online Stat Book* Available: http://onlinestatbook.com/2/estimation/proportion_ci.html.

[7]Fisher, R., Perkins, S., Walker, A., and Wolfart, E., "Hough Transform," *Image Processing Learning Resources* Available: http://homepages.inf.ed.ac.uk/rbf/HIPR2/hough.htm.